Theoretical and experimental description of the growth of GaAs and AlxGa1-xAs in the pulse reactor

Journal of Crystal Growth 102 (1990) 1–15
North-Holland

THEORETICAL AND EXPERIMENTAL DESCRIPTION OF THE GROWTH OF GaAs AND $Al_xGa_{1-x}As$ IN THE PULSE REACTOR

W.G.J.H.M. VAN SARK *, J. VAN SUCHTELEN, J.E.M. HOGENKAMP, M.H.J.M. DE CROON, R.A. VELTHUIS and L.J. GILING

Department of Experimental Solid State Physics, RIM, Faculty of Science, University of Nijmegen, Toernooiveld, 6525 ED Nijmegen, The Netherlands

Received 16 January 1990

The pulse reactor is a cyclic-operation low-pressure metalorganic vapour phase epitaxy (MOVPE) reactor in which in principle any binary, ternary, and quaternary multilayer device structure can be grown in a succession of a few thousands of "growth cycles". In each cycle, of typical duration ~1 s, growth proceeds from a low-pressure (~1 mbar) mixture that contains the necessary growth species and which during the reaction is immobile with respect to the substrates. In one cycle, 1 to 50 atomic layers can be deposited. A theoretical description of the evolution of the growth rate in one cycle is presented. In one cycle the growth rate determining mechanism changes from kinetically to diffusion controlled. A cold-walled version of the pulse reactor is now operational and has been tested for GaAs–$Al_xGa_{1-x}As$ growth. Growth rate (up to 50 μm/h) and morphological qualities are comparable to conventional MOVPE. In the present reactor uniformly is typically ~5% over a complete 2 inch wafer and can probably be improved easily.

1. Introduction

The most common problem encountered in continuous-flow metalorganic vapour phase epitaxy (MOVPE) reactors, which are used throughout the semiconductor industry for the fabrication of various opto-electronic devices, is the occurrence of the depletion effect [1–4]. The concentration of growth species diminishes along the direction of the flow, which results in a non-uniform thickness distribution. Solutions are possible, but generally still lead to inefficient use of the expensive metalorganic compounds. A sophisticated way of avoiding depletion is the use of a tilted susceptor [3]. In order to overcome the depletion problem in another way, a "Pulse Reactor" has been developed recently [5,6], which essentially is a conventional reactor provided with fast-acting valves at entrance and exhaust, and a vacuum pump.

Fig. 1 shows a block scheme of the essential parts of the pulse reactor. These are situated inside a glovebox in a purified N_2 atmosphere to avoid contamination of the reactor during loading of substrates. The growth of multilayer structures proceeds in growth cycles, in which two processes can be discerned that occur simultaneously: (1)

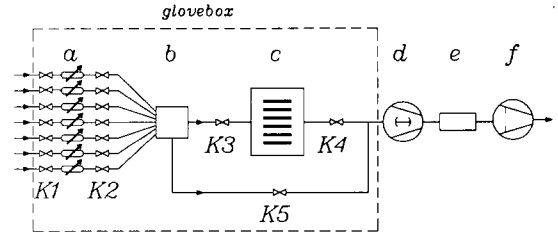

Fig. 1. Schematic block diagram of the pulse reactor system: (a) gas pipettes (0.1–2 cm^3, 1 bar); (b) mixing chamber (40 cm^3, 40 mbar); (c) reactor (1500 cm^3, 1 mbar); (d) Roots pump; (e) arsine cracker (4000 cm^3, 800 °C) and dust filter; (f) two-stage rotary pump. The "peristaltic" guidance of the gas mixture is controlled by valves K1 and K2 (7×), K3 and K4. Shunt valve K5 can be used for purging the mixing unit and in some failure modes.

* Present address: Department of Atomic and Interface Physics, Utrecht University, P.O. Box 80.000, 3508 TA Utrecht, The Netherlands.

reaction and (2) mixing. The growth cycle (i.e. reaction) starts with the evacuation of the reactor. Subsequently, the reactor is filled with the reactive gas mixture, which was prepared in the mixing chamber during the previous cycle, and is left closed for 1–2 s to allow the gases to react. Mixing of the growth gases takes place parallel to the reaction and is shorter in duration by definition. As the growth gases are introduced in a pulsed way, no massflow controllers can be used. Therefore a special gas introduction system has been developed [5], which in the present setup allows up to 7 gases to be used in the reactor. In the mixing process first the appropriate gases are introduced into the mixing chamber, one by one. The amount of gas can be varied by adjusting the volume of the gas pipettes and the inlet pressure of the growth gases. After mixing, the gases are introduced in the reaction chamber. The control of the complete Pulse Reactor system, comprising over 40 valves and various sensors and actuators to ensure safe, reliable, and reproducible operation, is automated using a microprocessor based industrial computer [6].

It has been pointed out previously [5], that the pulse reactor features several advantages over continuous-flow reactors. It is expected that a better uniformity of layers can be obtained, as flow is absent and the diffusivity of growth species at the mbar level is high. Sharp transitions are ensured in principle, because the growth proceeds in cycles during which 1–50 monolayers are deposited. The composition and thickness of the layer grown in each cycle – out of a total of thousands – can be programmed individually. This programmability and flexibility makes the pulse reactor suitable for techniques such as atomic layer epitaxy (ALE) [7]. The gas mixing system can work without a carrier gas, if required. Economy of metalorganics is ensured as the cycle duration can be chosen such that nearly all growth species have reacted. Of industrial importance is the fact that the pulse reactor can easily be scaled up to a multi-wafer reactor.

In this paper we present a theoretical description of the growth rate during a growth cycle as a function of time. Several stages can be distinguished: it will be shown that at the beginning of the cycle the growth is kinetically controlled and that after a certain time the diffusion of growth species is rate determining. The growth temperature greatly influences the relative duration of these stages. We furthermore report on experiments that have been carried out to determine the uniformity of grown layers of GaAs and $Al_xGa_{1-x}As$ as a function of reactor geometry. Also the dependence of the growth rate on the temperature and the crystallographic orientation of the substrate dependence of the growth rate are investigated. Earlier test results showing the possibilities and quality of the pulse reactor have been given elsewhere [6]. To date the reactor walls are cooled, which poses some problems related with diffusion of growth species towards the substrates. As the glovebox system could not be used yet with a hot-wall reactor and therefore purity conditions are far from ideal, we have focused on the geometrical aspect of thickness uniformity. Installation of a hot-walled reactor version will improve the layer quality and uniformity, which are nevertheless already good.

2. Growth rate during one cycle

The evolution of the growth rate during one reaction cycle can be divided into different stages. It will be shown in this section that in each stage the growth is limited by another mechanism. At time $t = 0$ the gas mixture is introduced into the reactor. Pressure and temperature equilibration takes between ~ 5 and ~ 50 ms, respectively, as deduced from pressure sensor measurements. In order to obtain layers that are homogeneous in thickness and composition, no deposition of importance should occur within this equilibration period. At the beginning of the reaction cycle, first species close to the substrate surface will decompose and diffuse to the substrate, where the growth reaction takes place. Subsequently, after a certain amount of time, the surface reaction will be rate limiting resulting in a more or less constant growth rate. Eventually, diffusion of growth species will be rate limiting, which results in an exponentially decreasing growth rate (cf. the depletion effect in horizontal MOVPE reactors [3,4]). It will be shown

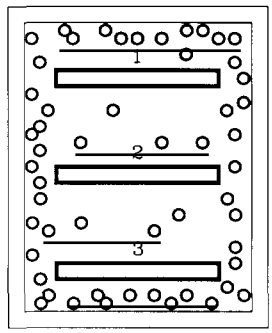

Fig. 2. Simplified view of the reactor chamber. The reactor wall is made of stainless steel (diameter 12.5 cm, height 12.5 cm) and is oil-cooled (300 K). The three molybdenum susceptors (diameter 6 cm) are resistance heated (typically 1000 K) and are placed equidistantly. Growth species (○) are concentrated near the cold wall, because of the Soret and Stefan effects.

that the durations of the various stages, that can be discerned in one reaction cycle, vary as a function of temperature through the temperature dependence of rate constants, which determine the CVD number. Besides this the growth rate is determined by the CVD number as well.

2.1. Simplified model

A quantitative and realistic description of the time evolution of the growth rate can be given with the use of the following overall reaction scheme [8]:

$$A(y, t) \overset{k_c}{\rightleftarrows} B(y, t) \overset{\text{diff.}}{\rightleftarrows} B(0, t) \xrightarrow{k_o} C(t) \qquad (1)$$

where $A(y, t)$, $B(y, t)$, and $C(t)$ are the concentrations of species A, B, and C, respectively, as a function of height y in the reactor and time t. A simplified view of the reactor is given in fig. 2. Three susceptors are placed equidistantly and are typically heated to 1000 K. Therefore the gas temperature between the susceptors is considered to be constant and equal to the susceptor temperature. The species A, B, and C may be identified as trimethylgallium (TMG), monomethylgallium (MMG), and GaAs, respectively. The growth of AlGaAs can be described with two of the above reaction schemes, one for GaAs and one for AlAs. The species A, B, and C for AlAs growth may be identified as trimethylaluminium (TMA), monomethylaluminium (MMA), and AlAs, respectively. Under the assumption that the temperature in the reactor is constant, the reaction where B is formed out of A takes place virtually everywhere in the reactor with reaction rate constant k_c [9,10]. Subsequently, species B diffuses from the bulk gas phase ($B(y, t)$) towards the surface ($B(0, t)$). The formation of C out of B at the substrate (positioned at the susceptor) is described with an overall reaction rate constant k_o, in which adsorption, desorption and incorporation processes are combined [8]. The growth of GaAs is treated as if only the diffusion of the Ga-containing species is important. This one component treatment generally is valid as AsH_3 is present in excess [1–4]. It should be noted that the diffusion of growth species is assumed to take place in one direction only (y). In reality this assumption will probably not be valid; however, the analysis of the one-dimensional case will already provide insight in the complex (three-dimensional) processes that occur in the reactor. Uniformity of the growth rate requires an axial diffusion field. A non-axial field can be forced into an axial field by placing a cylindrical diffusion shield on top of the susceptors, with the axis parallel to the direction of the normal of the susceptor. In the following the growth is described on the bottom susceptor.

We consider an axially symmetric cylinder of height h (= the distance between two susceptors, or the reactor height if only one susceptor is positioned at the bottom of the reactor) that is filled with growth species A and B. The height coordinate is denoted y. Growth takes place at the substrate surface, which is placed at $y = 0$. Growth species diffuse (diffusivity D_A, D_B) from the cylinder volume towards the substrate, where the growth reaction occurs. The temperature at the top of the cylinder equals the substrate temperature T_s, so no temperature gradient is present, hence thermal diffusion can be neglected and the reaction A → B occurs everywhere in the reactor volume. It should be noted that also at the top of the cylinder deposition will occur. In the reactor an excess AsH_3 is present, so that only the concentration of the group III component must be taken into account.

We assume that the cylinder is uniformly filled with component A at time $t = 0$. The input concentration of the growth species A is A_0. At $t = 0$ no B is present yet. We furthermore assume that the temperature of the input gas increases instantaneously from room temperature T_0 to T_s. The consequence of this assumption is that the duration of temperature and pressure equilibration is taken as infinitesimally small, i.e. 0 s. This is a rather rigourous assumption, it, however, facilitates the mathematical description considerably. As a consequence, the growth rates predicted by the model must be interpreted carefully when appreciable growth rates are computed for times smaller than ~ 50 ms, being the practical equilibration time.

The growth rate as a function of time $R(t)$ can be determined by solving the partial differential equations that hold for the concentration of species A and B. For species A we arrive at [11]:

$$\frac{\partial A(y, t)}{\partial t} = D_A \frac{\partial^2 A(y, t)}{\partial y^2} - k_c A(y, t), \tag{2}$$

with boundary conditions

$$\left.\frac{\partial A(y, t)}{\partial y}\right|_{y=0} = 0, \tag{3}$$

$$\left.\frac{\partial A(y, t)}{\partial y}\right|_{y=h} = 0, \tag{4}$$

$$A(y, 0) = A_0. \tag{5}$$

The solution for this partial differential equation is given by:

$$A(y, t) = A_0 \exp(-k_c t). \tag{6}$$

Note that $A(y, t)$ is independent of y, so that in the following $A(t)$ is used.

For species B the following partial differential equation has to be solved (the reaction B → C is accounted for in the boundary conditions):

$$\frac{\partial B(y, t)}{\partial t} = D_B \frac{\partial^2 B(y, t)}{\partial y^2} + k_c A(t) \tag{7}$$

The boundary conditions at the susceptor and top of the reactor are (using the dimensionless height $q = y/h$):

$$\left.\frac{\partial B(q, t)}{\partial q}\right|_{q=0} = \frac{k_{o,q=0} h}{D_B} B(0, t) = N_0 B(0, t), \tag{8}$$

$$-\left.\frac{\partial B(q, t)}{\partial q}\right|_{q=1} = \frac{k_{o,q=1} h}{D_B} B(1, t) = N_1 B(1, t), \tag{9}$$

$$B(q, 0) = 0. \tag{10}$$

Boundary conditions (8) and (9) were written in terms of the CVD number [12,13]:

$$N_{CVD,o,q=0} \equiv N_0 = k_{o,q=0} h / D_B, \tag{11}$$

$$N_{CVD,o,q=1} \equiv N_1 = k_{o,q=1} h / D_B. \tag{12}$$

In principle deposition will occur not only at the susceptor ($y = 0$), but also at the top of the reactor ($y = h$), as no temperature gradient is present. In practice the material of the top of the reactor (stainless steel or Mo heat shields at the backside of a susceptor situated above) differs from the material at the susceptor, i.e. GaAs. Therefore the reaction rate constant k_o may be different for $y = 0$ and $y = h$, which is represented by $k_{o,q=0}$ and $k_{o,q=1}$, and hence the different CVD numbers N_0 and N_1. Also for the reaction A → B a CVD number can be defined. It was shown elsewhere [9,10] that the rate constant k_c (expressed in 1/s) must be multiplied with a thickness corresponding to the thickness δ_r of the chemical boundary layer. This layer especially is present in MOVPE flow reactors, where strong temperature gradients are responsible for the fact that only in a thin layer just above the substrate surface the chemical reaction A → B will take place. The thickness of this chemical boundary layer in these cases is typically of the order of several mm [9,10]. In the pulse reactor, as a consequence of the constant temperature, this boundary layer is equal to the height of the reactor. The CVD number thus can be defined as follows:

$$N_c = k_c \delta_r h / D_A = k_c h^2 / D_A. \tag{13}$$

The concentration $B(y, t)$ is found by solving eq. (7) using Laplace transformation. Defining $\bar{B}(y, s)$ as the Laplace transform $\mathscr{L}(B(y, s))$ of $B(y, t)$, with transformation parameter s, we can write

$$s\bar{B}(y, s) = D_B \frac{\partial^2 B(y, s)}{\partial y^2} + k_c \bar{A}(s), \tag{14}$$

with $\bar{A}(t)$ the Laplace transform of $A(t)$, which follows from eq. (6):

$$\bar{A}(s) = \frac{A_0}{k_c + s} \tag{15}$$

Solving eq. (14) yields as general solution

$$\bar{B}(y, s) = \frac{k_c A_0}{(k_c + s)s} + \eta \sinh\left(\sqrt{\frac{s}{D_B}}\, y\right) + \theta \cosh\left(\sqrt{\frac{s}{D_B}}\, y\right), \tag{16}$$

with η and θ constants that are to be determined from the boundary conditions. Using the boundary conditions we finally arrive for $\bar{B}(y, s)$ at

$$\bar{B}(y, s) = \frac{k_c A_0}{(k_c + s)s}\left[1 + \frac{\eta'}{z} N_0 \sinh y' + (\eta' - 1)\cosh y'\right], \tag{17}$$

where the following substitutions have been used:

$$z = \sqrt{\frac{s}{D_B}}\, h, \tag{18}$$

$$y' = \sqrt{\frac{s}{D_B}}\, y, \tag{19}$$

$$\eta' = \frac{N_1(\cosh z - 1) + z \sinh z}{(N_0 + N_1)\cosh z + \dfrac{z^2 + N_0 N_1}{z}\sinh z}. \tag{20}$$

The growth rate in one cycle is determined from (note that also for the growth rate a Laplace transform is used)

$$\bar{R}(s) = k_{o,q=0}\bar{B}(0, s), \tag{21}$$

which yields from eq. (17):

$$\bar{R}(s) = \frac{k_{o,q=0} k_c A_0}{(k_c + s)s}\eta' \tag{22}$$

$$= \frac{N_0 N_c A_0 h}{(N_c + z^2)z^2}\eta', \tag{23}$$

where the definition of N_c through eq. (13) is used, as well as the assumption that $B_A = D_B$. Instead of being a function of axial distance as is the case in continuous-flow horizontal MOVPE reactors, the growth rate is a function of time. The growth species now will be depleted in time.

In order to find the inverse Laplace transform $\mathscr{L}^{-1}(\bar{R}(s))$, eq. (23) is approximated for small t ($\bar{R}_1(s)$) and large t ($\bar{R}_2(s)$). The transition from the solution for small t to the one for large t occurs around $t_t \sim h^2/D_B\pi$, as can be derived from inverse transformation of eq. (18). The development point marks the time where the concentration profile in the gas phase has been built up to the full height of the reactor. This development time is comparable to the entrance length for building up the concentration profile in continuous-flow reactors [3]. For the pulse reactor it effectively is the time needed to completely develop the diffusion profile over the whole height of the reactor. Note that the development time is independent of the chemistry in the gas phase or at the surface. For (very) small t, i.e. $z > 1$, the Laplace transform for the growth rate $\bar{R}_1(s)$ can be approximated as follows:

$$\bar{R}_1(s) = A_0 h \frac{N_0 N_c}{z(N_c + z^2)(N_0 + z)} \quad (z > 1). \tag{24}$$

Note that N_1 does not occur in this expression. For these small times the distance over which growth species can diffuse is smaller than the height h, so that perturbations resulting from deposition onto the top of the reactor are not noticed. For large t ($z < 1$) the following first order approximation can be derived for $\bar{R}_2(s)$:

$$R_2(s) = A_0 h \frac{N_0(1 + \frac{1}{2}N_1)}{N_0 + N_1 + N_0 N_1} \times \frac{1}{1 + z^2 f(N_0, N_1, N_c)} \quad (0 < z < 1), \tag{25}$$

where $f(N_0, N_1, N_c)$ is written as:

$$f(N_0, N_1, N_c) = \frac{1}{N_c} + \frac{\frac{1}{2}(N_0 + N_1) + \frac{1}{6}(N_0 N_1) + 1}{N_0 + N_1 + N_0 N_1} - \frac{\frac{1}{24}N_1 + \frac{1}{6}}{\frac{1}{2}N_1 + 1}. \quad (26)$$

The solution for the growth rate itself from these approximated Laplace transforms (eqs. (24) and (25)) can now be found [14].

For small t ($0 \leqslant tD_B/h^2 \leqslant \pi^{-1}$), we finally arrive at

$$R_1(t) = \frac{A_0 D_B}{h} \frac{N_0 N_c}{N_0^2 + N_c} \left\{ \exp(-N_c p) \times \left[\frac{2}{\sqrt{\pi}} \frac{N_0}{\sqrt{N_c}} \int_0^{\sqrt{N_c p}} \exp(\lambda^2)\, d\lambda - 1 \right] + \exp(N_0^2 p)\, \mathrm{erfc}\left(\sqrt{N_0^2 p}\right) \right\}, \quad (27)$$

where λ is an integration variable and where for convenience the dimensionless time $p = tD_B/h^2$ is introduced. The term between brackets contains Dawson's integral which is tabulated elsewhere [14] and varies between 0 and 1.

For large t ($\pi^{-1} < tD_B/h^2 \leqslant \infty$), the result is

$$R_2(t) = \frac{A_0 D_B}{h} \frac{N_0(1 + \frac{1}{2}N_1)}{N_0 + N_1 + N_0 N_1} \frac{1}{f(N_0, N_1, N_c)} \times \exp\left(- \frac{p}{f(N_0, N_1, N_c)} \right). \quad (28)$$

Note that in both equations still all kinetic processes are present (surface and gas phase reaction kinetics and diffusion). It will be shown in the following that depending on the actual values of N_0 and N_c, the growth rate determining mechanism either is the diffusion of growth species or surface/gas phase kinetics, respectively.

The total amount of species that is deposited in one cycle (= the thickness increment per cycle T_{cy}) can be determined by integrating over the cycle time t_{cy} (typically 1.5 s). We then find, using $t_t = h^2/D_B\pi$ as cross-over point for the time interval (see above),

$$T_{cy} = \int_0^{t_{cy}} R(t)\, dt = \int_0^{t_t} R_1(t)\, dt + \int_{t_t}^{t_{cy}} R_2(t)\, dt. \quad (29)$$

The maximum obtainable layer thickness per pulse is determined by $A_0 h$. Using the minimum possible mole fraction of TMG in H_2 ($\sim 10^{-3}$ in 1 bar H_2 input pressure in the smallest possible pipette volume) the obtained layer thickness per cycle equals ~ 0.1 nm, so that ALE is possible. If pure TMG is used – extracting it directly from the bottle with a vapour pressure of ~ 1000 Pa (bottle temperature 10 °C) and using the largest possible pipette volume – the thickness increment per cycle can be as much as 60 nm.

2.2. Calculation of the growth rate

In this section the evolution of the growth rate is computed, which is based on the various CVD numbers [12,13], as derived in the previous section. These CVD numbers represent the influence of either gas phase kinetics ($N_c = k_c h^2/D_A$) or the overall surface kinetics ($N_0 = k_{o,q=0} h/D_B$). The CVD number N_1 only is a special case of N_0, viz. it represents surface kinetics at the top of the reactor. In general, the growth rate is controlled by kinetics when the CVD number is smaller than 1, and it is diffusion controlled for values larger than 1. It will be shown that depending on the values of these three CVD numbers the rate controlling mechanism can be gas phase kinetics, surface kinetics, or diffusion.

We consider the growth to take place at a growth temperature of 700 °C. In atmospheric pressure MOVPE it was calculated that in this case the CVD number $N_c (= k_c \delta_r h/D_A)$, which belongs to the decomposition reaction in the gas phase, is of the order of 1000 [8] using data on the decomposition of TMG to MMG [15]. Here, the pressure in the pulse reactor is roughly 2 mbar, so that the diffusion constant D_A (or D_B) is more than two orders of magnitude larger than at atmospheric pressure. Besides this, the boundary layer thickness δ, equals the height h (= 4 cm), instead

of several mm. Hence, in this case the constant N_c – which is used in eq. (23) – is of the order of 300. We have used $D_B = 500$ cm^2/s (700 °C).

The CVD number N_0 was in atmospheric pressure MOVPE calculated to be in the range 0.1–10, depending on the temperature [8]. At a temperature of 700 °C it is expected to be of the order of 1, or somewhat smaller. Therefore, as regards the overall surface reactions we will consider three cases for the CVD number N_0: (i) $N_0 = 0.03$ (small k_o with respect to D_B/h, kinetically controlled), (ii) $N_0 = 3$ (transition region), and (iii) $N_0 = 300$ ($k_o > D_B/h$, diffusion controlled). Case (iii) is included for completeness. Each of these cases will be considered for the two extreme situations $N_1 = 0$ (no deposition at the top of the reactor), and $N_1 = N_0$ (deposition at the top of the reactor which is equal to the deposition on the substrate). The development time t_t ($= h^2/D_B\pi$), where the expression for the growth rate changes from $R_1(t)$ (eq. (27)) to $R_2(t)$ (eq. (28)), differs for the two different N_1 cases. In the case that $N_1 = 0$, t_t is calculated to be ~ 0.010 s ($t_t(a)$), using $D_B = 500$ cm^2/s and $h = 4$ cm. For $N_1 = N_0$ the reactor height h is effectively reduced by a factor of two, so that $t_t \sim 0.0025$ s ($t_t(b)$). We will see that in these short times the chemistry and diffusion in the gas phase rapidly are established with respect to the thermalization time.

(i) $N_0 = 0.03$. Fig. 3 shows the calculated growth rate $R(t)$ as a function of time for $N_1 = 0$ (curve a) and $N_1 = N_0$ (curve b). Note that $R(t)$ is made dimensionless by dividing by A_0D_B/h, being the maximum diffusion flux. Several regions in the growth curve can clearly be discerned, as is indicated in fig. 3. At small times (region I) the growth rate linearly increases in time. In this region the growth starts from the deposition of growth species which are present in the thin layer close to the surface, and is continued by the supply from species B which are created in adjacent gaseous layers and which thereafter diffuse to the surface. It is most easily shown, by using the Laplace transform of the growth rate, Eq. (24), that for these small times, i.e. for $z \gg N_0$, $N_c^{1/2}$, the growth rate is given by $R_1(t) = A_0k_ck_ot$. This explains the linear behaviour in the log-log plot of R_1 versus t. At $t = 10^{-4}$ s the creation of B in these adjacent

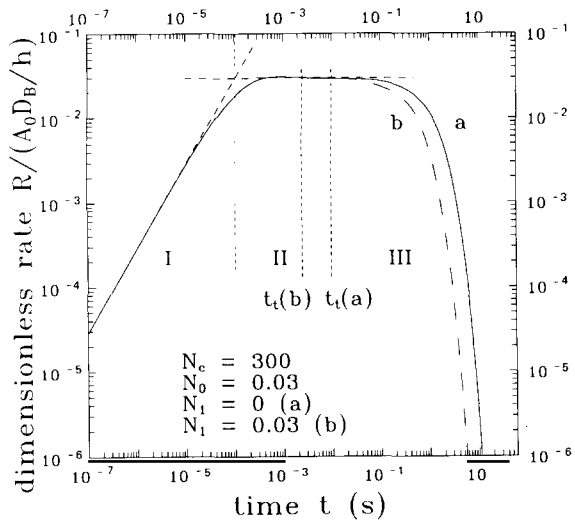

Fig. 3. Log-plot of the calculated dimensionless growth rate $R(t)h/A_0D_B$ in one reaction cycle as a function of time for $N_c = 300$, $N_0 = 0.03$, and (a) no deposition on the top wall ($N_1 = 0$) and (b) with deposition on the top wall ($N_1 = N_0$). Three regions, marked I, II and III, can be discerned, each dominated by a different process. The times t_t(a) and t_t(b) refer to the development time t_t (see text), which is different for $N_1 = 0$ (curve a) and $N_1 = N_0$ (curve b).

gas layers is almost completed, while the diffusion of B to the surface goes so fast that the surface chemistry becomes rate limiting (region II). This occurs for times $N_0 < z < N_c^{1/2}$ and as again directly follows from eq. (24), the growth rate in this region is given by $R_1(t) = A_0k_o =$ constant. The precise time where region I changes to region II is given by $t_{I-II} = 1/k_c = h^2/D_BN_c = 1.1 \times 10^{-4}$ s. The growth rate remains constant upto the development times $t_t(a)$ and $t_t(b)$, beyond which $R_1(t)$ no longer is valid, and the growth rate is determined by the expression for $R_2(t)$ (eq. (28)). From this equation it directly follows that for larger times $z < N_0$, $N_c^{1/2}$, the growth rate is given by $R_2(t) = A_0k_o \exp(-k_ot/h)$, which means that the exponential depletion of growth species starts to control the growth rate (region III). Note that in fig. 3 the exponential behaviour remains exponential because of the log-log plotting. The depletion in case of deposition on the top of the reactor (curve b) is stronger than in the case of no deposition on the top (curve a): the growth rate of course is lower in the former case. Note that for

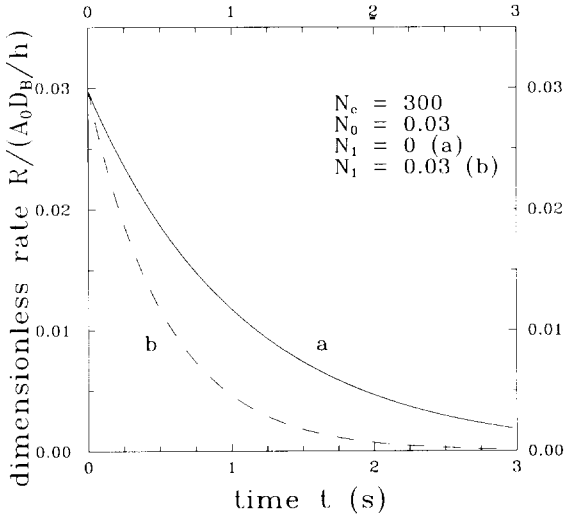

Fig. 4. Linear plot of the calculated dimensionless growth rate $R(t)h/A_0D_B$ in one reaction cycle as a function of time for $N_c = 300$, $N_0 = 0.03$, and (a) $N_1 = 0$ and (b) $N_1 = N_0$, illustrating the fact that the last region contributes the most to the total thickness increment.

small times (regions I and II) both curves a and b coincide, which also is clear from eq. (27), that is independent of N_1. It appears that the complete curves beyond these development points at 10 and 2.5 ms are determined by depletion of the gas phase. The length of regions II and III differ for the two curves a and b. From analysis it follows that the last stage in the reaction cycle has the largest contribution to the amount of deposited material, which is also illustrated in fig. 4, where the growth rate is plotted linearly versus time. The two initial regions I and II are so short that the fast rise from zero to the value $R(t)h/D_BA_0 = 0.03$ cannot be discerned. The complete curves effectively are described by the exponential depletion in this case. Calculation of the thickness increment between $t = 10$ ms and the cycle time of 1.5 s shows that about 75% of the total increment is grown in this last region. If the cycle time is increased to 2 s, this increment is increased to 85%. Under these conditions, i.e. $N_0 = 0.03$, the cycle time of 1.5 s may be somewhat too short.

We once more have to point out, that the calculated growth rate curves should be interpreted with care for times t smaller than the equilibration time which is ~ 50 ms. Practically the temperature of the introduced gases has to increase from room temperature to 700 °C. The CVD number N_c consequently will vary as a function of time. As N_c will be smaller than 300 for low temperatures (see also ref. [8]), the transition from the first stage to the second one will occur at a time larger than 0.1 ms as derived above, but probably smaller than 10 ms. This will not affect the obtained results on the growth rate evolution, as the last region in the reaction cycle, which starts for $N_0 = 0.03$ at 10 ms for $N_1 = 0$, and at 2.5 ms for $N_1 = N_0$, will have the largest contribution to the amount of deposited material. For larger values of N_0 (cases (ii) and (iii)) this conclusion may no longer be valid.

(ii) $N_0 = 3$. In fig. 5 the calculated dimensionless growth rate $R(t)h/A_0D_B$ is shown as a function of time again for $N_1 = 0$ (curve a) and $N_1 = N_0$ (curve b). It should be noted that the development times $t_t(a)$ and $t_t(b)$ have the same values as in the former case, as they are independent of the CVD numbers. As in the case of $N_0 = 0.03$, the transitions from one region to another can clearly

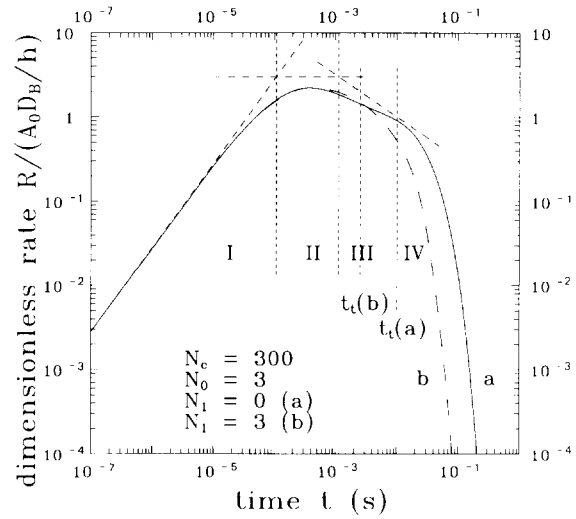

Fig. 5. Log-log plot of the calculated dimensionless growth rate $R(t)h/A_0D_B$ in one reaction cycle as a function of time for $N_c = 300$, $N_0 = 3$, and (a) $N_1 = 0$ and (b) $N_1 = N_0$. Four regions, marked I, II, III and IV, can be discerned, each dominated by a different process. The times t_t(a) and t_t(b) refer to the development time t_t (see text), which is different for $N_1 = 0$ (curve a) and $N_1 = N_0$ (curve b).

be discerned and they are indicated in fig. 5. Here, the first region also ends at 0.1 ms, after which the surface reaction becomes rate limiting at the constant level of $R_1(t) = A_0 k_o$. Due to the larger value of N_0, this second region now is shorter in length than in the former case (fig. 3). Because k_o is 100 times larger, the surface processes run quite fast, so fast that before the diffusion profile is fully developed, the supply from the gas phase becomes rate limiting. The condition $z < N_0$, $N_c^{1/2}$ now can be used in the equations for $R_1(t)$. From the Laplace transform of the growth rate $\bar{R}_1(s)$ as given by eq. (24) it follows immediately that $R_1(t)$ is given by $R_1(t) = A_0\sqrt{D_B/\pi t}$, resulting in a slope $-\frac{1}{2}$ in the log-log plot (region III). This region is determined by building up the diffusion profile. It appears that the growth species now have to come from so far, that the surface kinetics become faster than the supply from the gas phase. It should be noticed that the exact time for the transition from region II to region III is given by $t_{II-III} = D_B/\pi k_o^2 = h^2/\pi D_B N_0^2 = 1.1 \times 10^{-3}$ s. In the former case this point lies so far away in time that eq. (24) no longer is valid, i.e. in fig. 3 this diffusion behaviour is not to be seen, as depletion sets in before this point is reached. In region III the diffusion path of growth species still is smaller than the reactor height h. For the development time t_t the diffusion length equals the reactor height, hence effects of deposition on the top of the reactor on the growth rate at the susceptor are noticed from that time on. Beyong the turning points of the equations depletion again sets in as determined by $R_2(t)$ (region IV). The growth rate in the second region is two orders of magnitude larger than in the $N_0 = 0.03$ case, which is due to the value of N_0 itself, as $R_1(t)$ is linearly dependent on N_0 in this case (eq. (28)). Here also the last region of the reaction cycle (time depletion) will have the largest contribution to the amount of deposited material. Calculation of the thickness increment between $t = 10$ ms and $t = 1.5$ s shows that 97% of the total increment is grown in this last region. In fact, the cycle can be shortened, as the growth rate is negligible beyond $t = 0.16$ s. However, it should also be noted that a major part of the growth has occurred before temperature and pressure have equilibrated, i.e. before 50 ms. This means that quite a large amount of the deposition has occurred in an uncontrolled way.

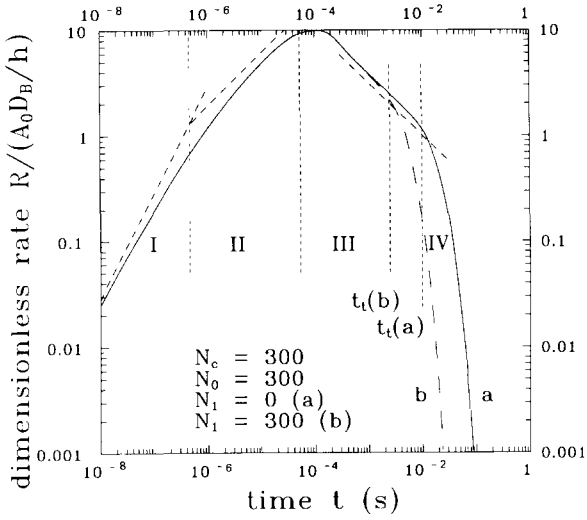

Fig. 6. Log-log plot of the calculated dimensionless growth rate $R(t)h/A_0D_B$ in one reaction cycle as a function of time for $N_c = 300$, $N_0 = 300$, and (a) $N_1 = 0$ and (b) $N_1 = N_0$. Four regions, marked I, II, III and IV, can be discerned, each dominated by a different process. The times t_t(a) and t_t(b) refer to the development time t_t (see text), which is different for $N_1 = 0$ (curve a) and $N_1 = N_0$ (curve b).

(iii) $N_0 = 300$. The calculated dimensionless growth rate $R(t)h/A_0D_B$ as a function of time is shown in fig. 6 for $N_1 = 0$ (curve a) and for $N_1 = N_0$ (curve b). The surface processes run so fast in this case that the whole deposition process takes place in the time needed for the equilibration of the gas. As it is assumed in these calculations that the equilibration process occurs infinitely fast, the process for this case still can be described theoretically. From eq. (24) and the fact that $N_c \ll N_0^2$, it can be deduced quite easily that we have three growth regions up to the development time t_t:

$$\text{(I)} \quad R_1(t) = A_0 k_c k_o t, \quad \text{as before,} \quad (30)$$

$$\text{(II)} \quad R_1(t) = 2A_0 k_c\sqrt{D_B t/\pi}, \quad \text{new,} \quad (31)$$

$$\text{(III)} \quad R_1(t) = A_0\sqrt{D_B/\pi t}, \quad \text{as before.} \quad (32)$$

Beyond t_t we additionally have in region IV:

$$\text{(IV)} \quad R_2(t) \approx 3\frac{A_0 D_B}{h}\exp\left(-3\frac{D_B t}{h^2}\right). \quad (33)$$

In the second region gas phase reactions coupled with diffusion now are rate limiting for the first time. This region sets in at $t_{I-II} = 4D_B/\pi k_c^2 = 4h^2/\pi D_B N_0^2 = 4.5 \times 10^{-7}$ s and ends at $t_{II-III} = 1/2k_c = h^2/2D_B N_c = 5.3 \times 10^{-5}$ s, where diffusion of growth species starts to be rate limiting. The slopes in fig. 6 do not correspond exactly with the ones predicted through eqs. (30)–(32), because of the fact that the approximations made in the derivation of these equations probably are too rigorous. Again, the effects of deposition on the top of the reactor are noticed beyond 2.5 ms. This last region will have the largest contribution to the amount of deposited material. The thickness increment between $t = 10$ ms and $t = 1.5$ s is calculated to be 97% of the total increment. For times t larger than 50 ms the growth rate is negligible. Thus under these conditions ($N_0 = 300$) nearly all growth species have been incorporated in the growing substrate within the time needed for equilibration. Therefore the calculation of the growth rate must be interpreted with great care.

2.3. Practical considerations

It is clearly seen in figs. 3–6 that the different growth conditions have a rather drastic effect on the evolution of the growth rate during one cycle, which will influence the relative importance of the kinetics and diffusion. High CVD numbers lead to much higher growth rates than low CVD numbers, while for low CVD numbers the growth cycle should be extended so as to use all the available growth species. The value of the CVD numbers can be manipulated by changing the growth temperature, as the rate constants k_c and k_o are strong functions of temperature. It is expected that the actual situation probably will lie in between cases (i) and (ii). It was found experimentally that the growth rate per cycle for a 1.5 s cycle was only a few percent smaller than for a 2 s cycle, i.e. not all growth species have reacted within 1.5 s. Therefore the CVD number N_0 must be larger than 0.03. The consequence is that most probably a large part of the actual growth process is taking place before the gas mixture has adjusted its pressure and temperature (50 ms). In order to lengthen the growth process, the value of N_0 (i.e. k_o) should be made smaller. This can be achieved by lowering the deposition temperature, but this normally leads to bad morphologies. A better way seems to be to raise the temperature. This also will ultimately lower the value of k_o, as k_o is composed of various surface properties of which especially the surface coverage is important. This coverage is a strong function of temperature such that at high temperatures the coverage goes to zero (cf. the diminishing growth rate of GaAs at temperatures $T > 700\,^\circ$C, which is due to desorption of Ga species from the surface [8]).

It should be borne in mind that the derived theory represents an ideal situation, without accounting for temperature and pressure equilibration. In practice not only diffusion of growth species in the y direction will occur, but also diffusion parallel to the substrate. Furthermore temperature gradients will be present, which increases thermal diffusion. Nevertheless, this theoretical description shows that kinetic and diffusion effects simultaneously occur in one reaction cycle. A simple Arrhenius plot of growth rate versus temperature therefore will not give a straight line in general.

In practice, the mechanisms predominant in the last stage will lead to non-uniform growth unless special measures are taken. Non-uniformity can be eliminated by a molybdenum shield designed to align the diffusion field in the axial direction (y). It will be shown that with such a shield, it is easy to obtain a homogeneity of better than 5% over a 2 inch wafer.

The duration of the stages largely depends on temperature, reactor geometry, and susceptor area and configuration. At a growth temperature of 700 °C, all stages will occur within one cycle of ~ 1–2 s. At lower (and higher) growth temperatures the CVD number N_0 will be smaller, so that the last stage may not be reached. During this last stage the Soret effect (thermal diffusion) and Stefan flow [11] can be important factors in the diffusion mechanism. High temperature gradients, which can be present in the mixture of H_2 and heavy molecules (TMG, TMA, and arsine) will lead to thermal diffusion, which may well lower the growth rate with 40–50% [4]. Moreover, edge effects, such as an increased growth rate at the

edges with respect to the growth rate in the center of the susceptor, will be present. Also the V/III ratio may decrease during one cycle, due to the radial outflow of As_n species and H_2 ("Stefan wind"). These factors will contribute to the inhomogeneity of the layer, especially in the case of a cold-walled reactor, because the majority of reactive mass will be concentrated near the cold wall in that case. Especially solid As is deposited during the growth run upon the cold walls, which makes it necessary to clean the walls after each growth run. During cleaning and loading, impurities are adsorbed on the walls. Because of the long desorption period, the grown layers – especially Al containing layers – are contaminated with oxygen. Increasing the temperature of the reactor wall to 300–400 °C will reduce the importance of Soret and Stefan diffusion, and therefore the risk of contamination is diminished as well. A hot-walled version of the pulse reactor will be installed shortly.

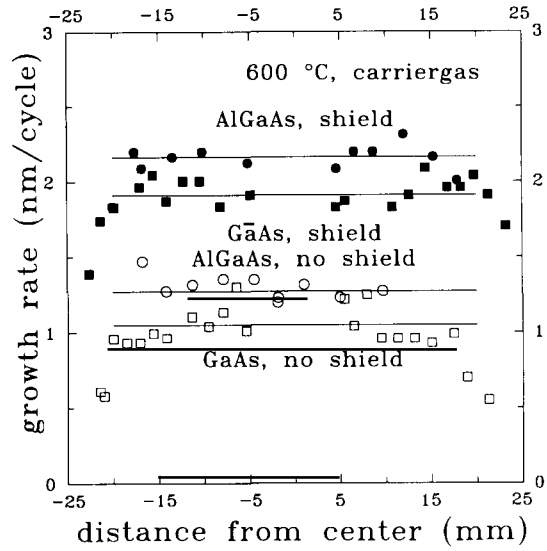

Fig. 7. Measured growth rates of GaAs and $Al_{0.3}Ga_{0.7}As$ as a function of the distance from the center of the susceptor, showing the effect of a diffusion shield at a growth temperature of 600 °C. The drawn lines correspond to the average growth rate for 80% of the susceptor width.

3. Experimental results

3.1. Conditions

A number of growth runs have been performed in order to investigate the uniformity of the growth rate over a complete 2 inch GaAs wafer in dependence of temperature and substrate orientation. A simplified sketch of the reactor chamber is shown in fig. 2, where the positions of the three suceptors used in this study are indicated. The (100) GaAs substrates (misoriented 0.25°, 2° and 4° off towards (110)) were placed on susceptors #2 and #3, which are resistance heated to the desired growth temperature (600–750 °C). Susceptor #1 was always heated to 400 °C. The temperature distribution around susceptor #3 is therefore different from the one around #2. Thermal diffusion effects are expected to be more important for susceptor #2 than for #3. The cylindrical diffusion shield was mounted on susceptor #3. TMG and TMA were introduced in the mixing chamber by either bubbling hydrogen through the liquids, which were held at 10 and 17 °C, respectively, or using the vapour pressure of the MO liquids. Pure arsine was led through a molecular sieve, prior to introduction in the mixing chamber. Hydrogen carrier gas was purified by passing it through a Pd purifier. The water content in the gas system was lower than 0.1 ppm. The pipette settings were such that the input partial pressures of the group III and V elements were fixed: $P_{TMG+TMA} = 110$ mbar, V/III = 15 (AlGaAs growth), and $P_{TMG} =$ 160 mbar, V/III = 12 (GaAs growth). The layers were grown employing typically 1000 growth cycles of duration 1 s ensuring that the layer thickness was a few μm. The growth rate was determined by examining scanning electron microscopy (SEM) images of stained cross-sections of grown epitaxial layers.

3.2. Influence of diffusion shield and growth temperature

For four growth temperatures (600, 650, 700, and 750 °C) the uniformity of the growth rate, with (susceptor #3) and without (susceptor #2) the diffusion shield, is shown in figs. 7–10 for GaAs and AlGaAs. In all cases hydrogen was

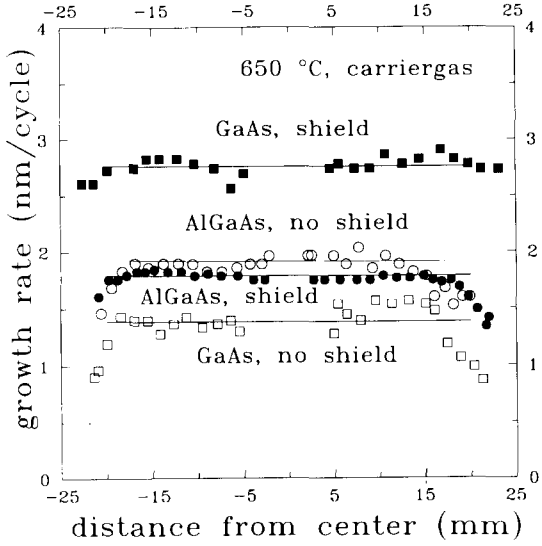

Fig. 8. Measured growth rates of GaAs and $Al_{0.3}Ga_{0.7}As$ as a function of the distance from the center of the susceptor, showing the effect of a diffusion shield at a growth temperature of 650 °C. The drawn lines correspond to the average growth rate for 80% of the susceptor width.

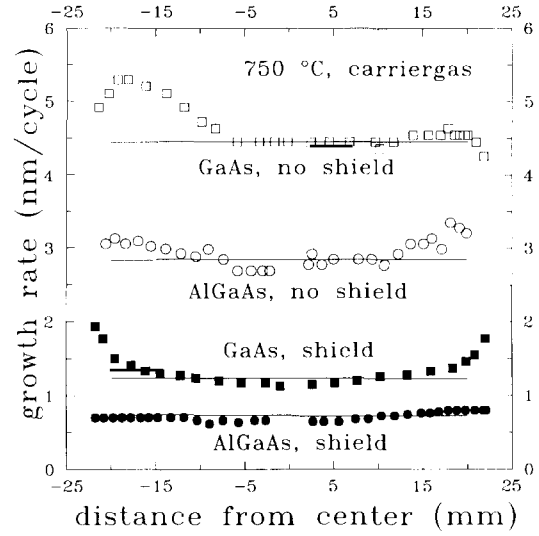

Fig. 10. Measured growth rates of GaAs and $Al_{0.3}Ga_{0.7}As$ as a function of the distance from the center of the susceptor, showing the effect of a diffusion shield at a growth temperature of 750 °C. The drawn lines correspond to the average growth rate for 80% of the susceptor width.

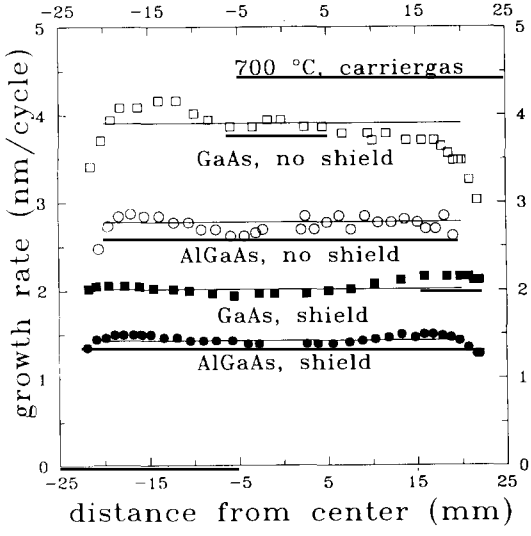

Fig. 9. Measured growth rates of GaAs and $Al_{0.3}Ga_{0.7}As$ as a function of the distance from the center of the susceptor, showing the effect of a diffusion shield at a growth temperature of 700 °C. The drawn lines correspond to the average growth rate for 80% of the susceptor width.

used as carrier gas. The substrates used were (100) GaAs 0.25° of towards (110). The diffusion shield indeed improves the uniformity both for GaAs and AlGaAs, especially side effects are eliminated by forcing the diffusion to proceed axially. This improvement is more pronounced at higher growth temperatures, which indicates that at these temperatures diffusion of growth species imposes a higher resistance than surface kinetics. The excellent uniformity which is achieved is the more impressive, if seen in the light of the dimensions of the heaters and samples. The 2 inch wafers are positioned on the 6 cm cross-section heaters, so that only a rim of 4–5 mm exists in these cases and large thermal gradients will be present at the rin of the heaters. For a growth temperature of 600 °C the uniformity without the diffusion shield is good, which is to be expected as at this low growth temperature kinetics are rate limiting.

Figs. 11 and 12 show the temperature dependence of the growth rate of GaAs and AlGaAs, determined from averaging the data of figs. 7–10. The error bars correspond to the maximum and minimum of the growth rate. Both for GaAs and AlGaAs the tendency is the same: at lower tem-

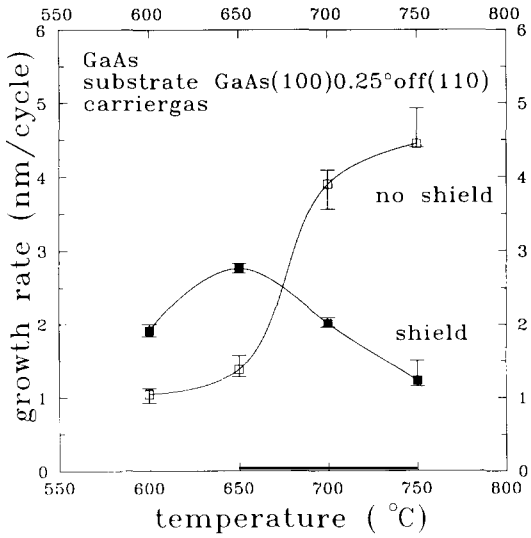

Fig. 11. Growth rates of GaAs as a function of growth temperature, averaged from figs. 7–10 for susceptor #2 (no shield) and #3 (shield). Variations in growth rate are indicated by error bars.

perature the growth rate obtained at susceptor #3 (shield) is higher than the growth rate at susceptor #2 (no shield), whereas this situation is reversed at higher temperatures. At lower temperatures thermal diffusion effects for susceptor #2 lead to a growth rate that is lower than for susceptor #3, where thermal diffusion hardly will play a role of importance as no temperature gradient (or only a small one) is present between the bottom of susceptor #2 and the top of susceptor #3. Growth will also occur at the bottom of susceptor #2, but the growth rate is small at low temperatures. At higher growth temperatures deposition on the bottom of susceptor #2 will be enhanced, thereby lowering the growth rate at susceptor #3, which was predicted in the model. In other words, susceptor #2 acts as a sink for growth species. Because of the presence of the diffusion shield, the growth at susceptor #3 can be described by the growth model, which was derived in the previous section. It was shown that for low values of the CVD number N_0 the growth rate per cycle is lower than for high values. The growth at susceptor #2 cannot be described with the growth model, because not only axial diffusion occurs but also diffusion parallel to the susceptor.

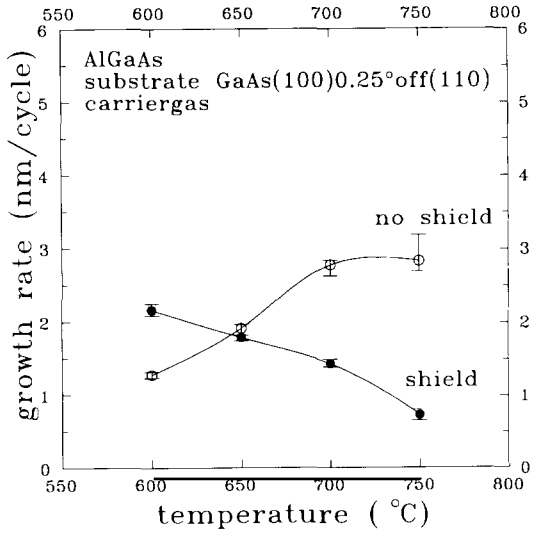

Fig. 12. Growth rates of $Al_{0.3}Ga_{0.7}As$ as a function of growth temperature, averaged from figs. 7–10 for susceptor #2 (no shield) and #3 (shield). Variations in growth rate are indicated by error bars.

In conclusion, it is shown that excellent uniformity can be obtained (better than 5%) if a diffusion shield is used at growth temperatures (700 °C) and rates (7 μm/h) comparable to conventional MOVPE reactors.

3.3. Bragg reflector

An elegant way to demonstrate the obtainable growth rate uniformity of the pulse reactor is the growth of high-reflectivity mirrors (Bragg reflectors), which find application in the fabrication of surface emitting lasers [16–19]. These reflectors consist of a periodic multilayer structure with alternating high (GaAs) and low (AlGaAs) refractive index materials. This quarter-wavelength structure exhibits high reflectivity over a limited wavelength around a central wavelength λ_c, which can be written as [17]

$$\lambda_c = 2(n_{GaAs}d_{GaAs} + n_{AlGaAs}d_{AlGaAs}) \qquad (34)$$

with n_i the refractive index and d_i the thickness of the individual layers. Mirrors with near 100% peak reflectivity at λ_c between 0.6 and 1.2 μm have been grown by MOVPE [16–18]. Colour

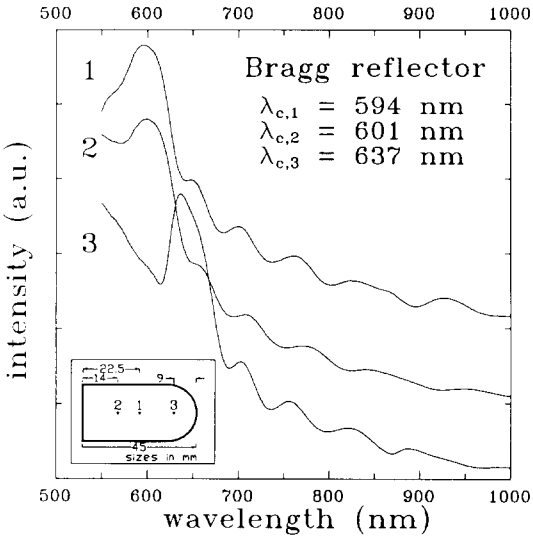

Fig. 13. Reflectivity as a function of wavelength of a GaAs/$Al_{0.41}Ga_{0.59}As$ Bragg reflector measured at three different positions at the sample (see inert). The GaAs layers have a thickness of 35 nm, whereas the AlGaAs layers are 40 nm thick. The surface of the multilayer structure appears to be yellowish (λ_c = 594–601 nm) over 80% of the sample to reddish (λ_c = 637 nm) at one side end.

differences (i.e. locally different λ_c) in Bragg reflectors with λ_c in the visible region can be used to determine growth rate uniformity in an easy and non-destructive way, as these differences correlate directly to local variations in the optical, and thus layer thicknesses. A multilayer structure consisting of 20 layer pairs of GaAs and $Al_{0.41}Ga_{0.49}As$, with individual thicknesses of 35 and 40 nm, respectively, was grown at a temperature of 700 °C at susceptor #3. Visual inspection of the grown layers showed that a large part of the sample appeared yellowish. At one side the colour was more reddish. Reflectivity measurements as a function of wavelength performed at three different positions at the sample are shown in fig. 13, confirming the visual inspection results. At position 3 the position of λ_c is shifted to longer wavelengths compared with positions 1 and 2, because of the fact that the layers are somewhat thicker towards the sides of the susceptor. It is clear that the results obtained here confirm the observations made previously, and that sophisticated structures can easily be grown in the pulse reactor.

3.4. Influence of misorientation and carrier gas

If surface kinetics are important, the growth rate will depend on the number of available step sites: the larger the number of steps, the larger the growth rate will be. The number of steps is determined by the misorientation of the substrates. It appears that at lower growth temperatures (650 °C) the growth rate is a slight function of misorientation, as is shown in fig. 14. Therefore, it is concluded that surface kinetics is an important factor at this growth temperature. Also shown in fig. 14 is the effect of using or not using hydrogen as a carrier gas. For all misorientations the growth rate without carrier gas is larger than with carrier gas. Hydrogen is active in the surface chemistry: it plays a role in the formation of methane from the metalorganics. Furthermore hydrogen determines diffusion phenomena through the (binary) diffusion coefficient, Soret and Stefan effects. If hydrogen is not used as carrier gas, the diffusion of TMG and TMA occurs in AsH_3. The diffusion coefficient then may be a factor of 10 lower in this case, which lowers the growth rate. On the other hand, the absence of hydrogen may enhance the decomposition of the metalorganics, which leads to an increase of the growth rate. Therefore it is

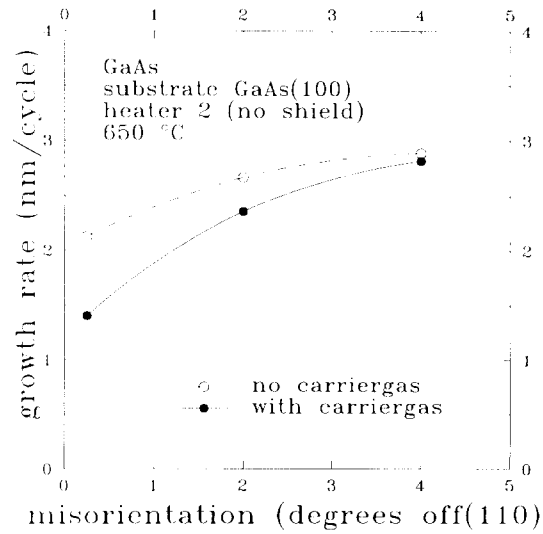

Fig. 14. Growth rates as a function of substrate misorientation at a growth temperature of 650 °C using either hydrogen as carrier gas or no carrier gas at all.

not clear a priori, what the exact effect is of not using a carrier gas. From our results (fig. 14) it appears that the growth rate is increased in this case. Therefore the kinetic phenomena are considered to be more important at this temperature, however, the orientation dependence is less pronounced.

4. Conclusion

The growth of GaAs and $Al_xGa_{1-x}As$ in the recently developed pulse reactor has been investigated as a function of temperature and reactor geometry. It was found that over a complete 2 inch GaAs substrate the variation of the growth rate is less than 5%. In order to achieve this a diffusion shield must be used to align the diffusion field in the axial direction. For this case a growth model was derived, that describes the growth evolution within a growth cycle. The model is used qualitatively, as various parameters are not known. In one cycle both kinetics and diffusion occur. Depending on the growth conditions – especially temperature – the relative importance of kinetics and diffusion varies. The excellent growth rate uniformity was also demonstrated by the growth of a Bragg reflector, with a central wavelength in the visible region. Over a large part of the reflector the apparent surface colour was the same. Future research will focus on the fabrication of laser structures.

Acknowledgements

This work was performed as a part of the research programme of the Netherlands Technology Foundation (STW) with financial support from the Netherlands Organization for Scientific Research (NWO).

References

[1] M.J. Ludowise, J. Appl. Phys. 58 (1985) R3.
[2] T.F. Kuech, Mater. Sci. Rept. 2 (1987) 1.
[3] J. van de Ven, G.M.J. Rutten, M.J. Raaijmakers and L.J. Giling, J. Crystal Growth 76 (1986) 352.
[4] W.G.J.H.M. van Sark, G. Janssen, M.H.J.M. de Croon and L.J. Giling, Semicond. Sci. Technol. 5 (1990) 16.
[5] J. van Suchtelen, J.E.M. Hogenkamp, W.G.J.H.M. van Sark and L.J. Giling, J. Crystal Growth 93 (1988) 201.
[6] W.G.J.H.M. van Sark, J.E.M. Hogenkamp, J. van Suchtelen and L.J. Giling, Rev. Sci. Instr. 61 (1990) 146.
[7] C.H.L. Goodman and M.V. Pessa, J. Appl. Phys. 60 (1986) R65.
[8] W.G.J.H.M. van Sark, M.H.J.M. de Croon and L.J. Giling, J. Appl. Phys., submitted.
[9] M.H.J.M. de Croon and L.J. Giling, Progr. Crystal Growth Characterization 19 (1989) 125.
[10] W.G.J.H.M. van Sark, M.H.J.M. de Croon, G. Janssen and L.J. Giling, Semicond. Sci. Technol., in press.
[11] R.B. Bird, W.E. Stewart and E.N. Lightfoot, Transport Phenomena (Wiley, New York, 1980).
[12] C.H.J. van den Brekel, Philips Res. Rept. 32 (1977) 118.
[13] C.H.J. van den Brekel and J. Bloem, Philips Res. Rept. 32 (1977) 134.
[14] M. Abramowitz and I.A. Stegun, Handbook of Mathematical Functions (Dover, New York, 1972).
[15] M. Suzuki and M. Sato, J. Electrochem. Soc. 132 (1985) 1684.
[16] R.L. Thornton, R.D. Burnham and W. Streifer, Appl. Phys. Letters 45 (1984) 1028.
[17] R. Beats, P. Demeester and P.E. Lagasse, J. Appl. Phys. 62 (1987) 723.
[18] A. Ibaraki, K. Kawashima, K. Furusawa, T. Ishikawa, T. Yamaguchi and T. Niina, J. Crystal Growth 93 (1988) 809.
[19] W. Wang, M.T. Pang, K. Komori, K.S. Lee, S. Arai and Y. Suematsu, Japan. J. Appl. Phys. 27 (1988) L1313.